

## Quantum-based microwave power measurements: Proof-of-concept experiment

T. P. Crowley,<sup>a)</sup> E. A. Donley, and T. P. Heavner

*National Institute of Standards and Technology, 325 Broadway, Boulder Colorado, 80305*

(Received 9 March 2004; accepted 26 April 2004; published 27 July 2004)

We present an initial proof-of-concept experiment to measure microwave power based on quantum-mechanical principles. Ground-state cesium atoms exposed to microwaves at 9.192 631 770 GHz oscillate between two hyperfine states at a rate that is proportional to the rf magnetic field strength. This provides a quantum-based method of measuring rf field strength that depends only on the fundamental parameters in the proportionality constant. A small fountain apparatus was used to prepare laser-cooled cesium atoms in a single hyperfine state, which were then launched through a cylindrical cavity operating in the TE<sub>011</sub> mode. After passing through the cavity, the fraction of atoms in the two hyperfine states was measured. Rabi oscillations between the two states were observed as a function of microwave field strength. The scaling with field strength and with time in the cavity agreed with theory to within 0.4%. The field strength in the cavity was used, together with measured  $S$  parameters, to determine the microwave power incident at a reference plane outside the fountain apparatus. The difference between the quantum-based microwave power measurement and a traditional microwave power measurement was less than 5% of the measured power. [DOI: 10.1063/1.1771501]

### I. INTRODUCTION

The most accurate methods for measuring microwave power are based on the principle of dc substitution.<sup>1</sup> The primary national standards at the National Institute of Standards and Technology (NIST) for measuring radio-frequency (rf) power are calorimeters and bolometric detectors that compare the heat produced by rf power with that produced by dc power. The standard uncertainties range from 0.12% at 50 MHz to 1.3% at 50 GHz, and are dominated by differences in the rf and dc heat dissipation processes. To obtain lower uncertainties will probably require development of techniques that do not rely on dc substitution.

Standards that are traceable directly to fundamental atomic processes have greatly increased the accuracy of measurements in areas such as time, frequency, and dc voltage, and have led to new applications. Similar capabilities in microwave amplitude measurements could potentially revolutionize microwave measurements and techniques.

The measurements presented here are based on the response of a cesium atom to an applied rf magnetic field.<sup>2</sup> Figure 1(a) shows the hyperfine levels of a cesium atom's  $6^2S_{1/2}$  electronic ground state and its  $6^2P_{3/2}$  electronic excited state. The hyperfine levels have small energy shifts relative to each other that depend on the total angular momentum quantum number  $F$ . The atomic nucleus has a spin angular momentum of  $7\hbar/2$ , while the outermost electron has a spin angular momentum of  $\hbar/2$ , where  $\hbar = h/2\pi$ , with  $h$  being Planck's constant. For the ground state, there are two possible values for the total angular momentum of the atom.

The lower  $F=3$  energy state has nuclear and electron spins that are antiparallel so that the total angular momentum is  $3\hbar$ . The higher energy  $F=4$  state has parallel nuclear and electron spins and a total angular momentum of  $4\hbar$ .

Associated with the spin of a particle is a magnetic moment and a magnetic field. The magnetic field produced by the outer electron interacts with the magnetic moment of the nucleus, and vice versa. This interaction causes the potential energy difference between the  $F=3$  and  $F=4$  states, which is called the hyperfine splitting due to its small size. With no external magnetic field, the energy difference is  $hf_{\text{HFS}}$ , where the hyperfine splitting frequency  $f_{\text{HFS}}$  is equal to 9.192 631 770 GHz. When an external dc magnetic field is applied, the states within the  $F=3$  and  $F=4$  groups are further split in energy, depending on  $m_F$ , the projection of the atom's angular momentum along this dc field. For weak dc field strength, the energy of the  $m_F \neq 0$  states vary linearly with applied field, while the  $m_F=0$  states are to the first order insensitive to magnetic fields and vary quadratically with applied field. In these experiments, a weak dc magnetic field is present that is strong enough to clearly separate the various  $m_F$  states, but which is not strong enough to make a significant change in the  $m_F=0$  energy. We examined transitions between the two  $m_F=0$  states.

Transitions between two quantum states can be induced by applying radiation at a frequency  $f = \Delta W/h$ , where  $\Delta W$  is the energy difference between the states. Radiation at frequency  $f_{\text{HFS}}$  will therefore cause cesium atoms to oscillate between the  $|F=3\rangle$  and  $|F=4\rangle$  states at a rate known as the Rabi frequency  $\Omega_R$ , given by

<sup>a)</sup> Author to whom correspondence should be addressed; electronic mail: crowley@boulder.nist.gov

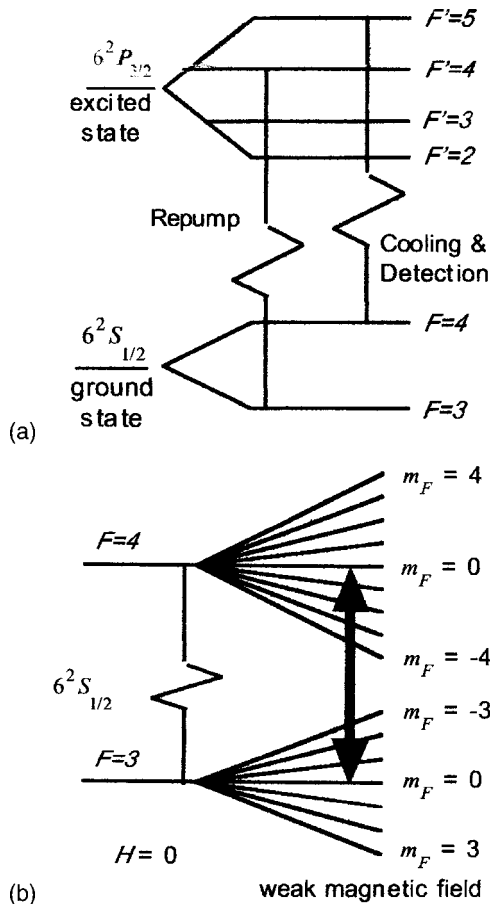


FIG. 1. (a) Schematic diagram of the hyperfine levels of the ground state and an electronic excited state of a cesium atom showing the cooling and repump transitions. (b) Detailed view of the ground-state energy levels. The large arrow indicates the transition used to measure the Rabi oscillations. In both (a) and (b), the energy of the levels increases from bottom to top, but the vertical axis is not to scale.

$$\Omega_R = \frac{\mu_0 \mu_B g_J M H_{rf}}{\hbar}, \quad (1)$$

where  $\mu_0$  is the permeability of free space,  $\mu_B$  is the Bohr magneton ( $9.27 \times 10^{-24}$  J/T),  $M$  is the quantum-mechanical matrix element  $\langle F, m_F | J_z | F+1, m_F \rangle$ ,  $J_z$  is the component of the electron angular momentum parallel to the dc magnetic field,  $g_J$  is equal to the electron  $g$  factor in this experiment, and  $H_{rf}$  is the amplitude of the rf magnetic field. The objective of this experiment is to determine  $H_{rf}$  by measuring the number of atoms in the  $|F=3, m_F=0\rangle$  and  $|F=4, m_F=0\rangle$  states after exposure to resonant microwaves.

The experiment is a proof-of-concept demonstrating that microwave amplitude (i.e., power) measurements based on a quantum standard are possible. No attempt has yet been made to address all of the issues required to implement this scheme as a national standard for microwave power. The experiments were conducted using a small cesium-fountain apparatus that was designed for use as a frequency standard.<sup>3</sup> Consequently, the apparatus is not optimized for microwave power measurements, and this affects the measurement accuracy that can be achieved. Abbreviated versions of our results

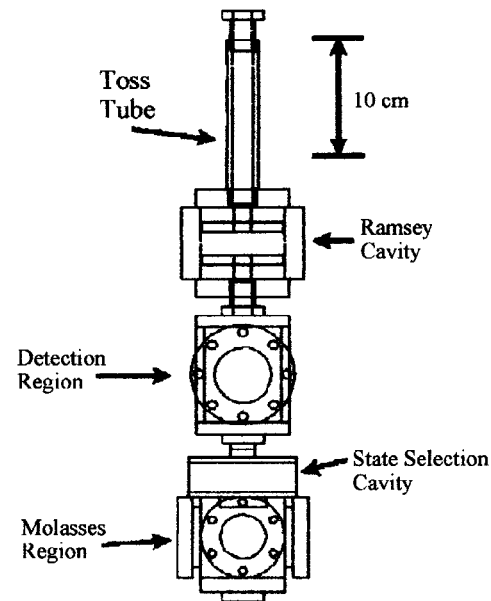


FIG. 2. Cesium-fountain vacuum chamber

were presented previously.<sup>4,5</sup> This article contains a more complete description of the technique and a more detailed explanation of our results.

An experiment similar to the one presented here was previously reported by the National Research Council in Canada.<sup>6</sup> In that experiment, laser-cooled rubidium atoms were exposed to a 6.8345 GHz microwave pulse emanating from an open-ended waveguide outside of the vacuum chamber. A series of measurements with different pulse lengths was made and the number of atoms that changed state after each pulse was recorded. The Rabi frequency for a given power level was determined by fitting the data to a cosine function. This was repeated for several different power levels. As expected, the Rabi frequency was found to scale linearly with the square root of the microwave power.

Our experiment's main advantage is that the fields in our cavity structure can be more accurately approximated than the fields in front of an open-ended waveguide in a laboratory. As a result, we are able to make an absolute comparison between a traditional microwave measurement and the Rabi oscillation measurement. Unfortunately, the uncertainties in this comparison are of the order of 30%. Another difference is that we pulse the field spatially instead of temporally. The exposure time cannot be conveniently changed in our apparatus, so we observe Rabi oscillations corresponding to changes in field strength rather than changes in exposure time. The two experiments were also performed with different atoms, and therefore at different frequencies.

## II. APPARATUS

### A. Fountain apparatus

A diagram of the cesium-fountain apparatus is shown in Fig. 2. A group of approximately  $10^8$  cesium atoms at a temperature of a few microkelvin was trapped and cooled using a vapor-cell magneto-optical trap (MOT) and an optical molasses (further described below). The MOT consists of six laser beams that intersect at the center of a dc magnetic

trap formed by a pair of anti-Helmholtz coils. The laser beams are tuned to the cooling resonance illustrated in Fig. 1(a). The frequency and polarization of the laser beams is set such that the Zeeman shift creates a position-dependent force that collects atoms from the background vapor, cools them, and pushes them toward the null in the magnetic field at the trap center. After collecting the atoms in the MOT for about 300 ms, the anti-Helmholtz magnetic field is turned off and the atoms are further cooled in an optical molasses.<sup>7</sup> With this magnetic field off, the atoms are not spatially confined, but their motion is inhibited by the laser forces. The term “optical molasses” is used to describe this slowing process since it is similar to the effect of a very viscous medium. The atoms are launched vertically in 1 ms by shifting the relative frequency between the upward- and downward-traveling laser beams. The atoms are subsequently cooled in the moving frame for 2 ms before the beams are turned off, and the atoms exhibit a fountain motion under the influence of gravity. The atoms are evenly spread among the nine magnetic sublevels ( $m_F = -4$  to  $+4$ ) of the  $|F=4\rangle$  hyperfine level of the  $6^2S_{1/2}$  ground-state, shown in Fig. 1(b).

After launching, the atoms first encounter a rectangular state-selection cavity operating in the  $TE_{104}$  mode. The frequency of the microwaves in the cavity is set to  $f_{\text{HFS}}$ . A small dc magnetic field is present from this cavity to the top of the fountain. This field breaks the degeneracy between the magnetic sublevels in each  $F$  state such that the  $|F=4, m_F=0\rangle$  to  $|F=3, m_F=0\rangle$  transition is probed without the interference of the other magnetic sublevels. These transitions are indicated by the heavy arrow in Fig. 1(b). This is the same transition used by atomic clocks, which are based on the ability to make high-precision measurements of  $f_{\text{HFS}}$ . The state-selection cavity is a preparatory stage in which the microwave amplitude is adjusted to maximize the transition probability from the  $|F=4, m_F=0\rangle$  to the  $|F=3, m_F=0\rangle$  state. All remaining atoms in the  $|F=4\rangle$  states are then removed using a pulse of light resonant with the  $|F=4, m_F\rangle \Rightarrow |F'=5, m_F\rangle$  transition, which is the same transition that was used to cool the atoms. The  $|F'=5\rangle$  state is a hyperfine sublevel of the  $6^2P_{3/2}$  excited electronic state.

The state-selected  $|F=3, m_F=0\rangle$  atoms then pass through the Ramsey cavity. This is where the quantum-based measurements are performed. Microwaves in the Ramsey cavity excite the same transition as the state-selection cavity. The Ramsey cavity is cylindrical, with a height of 1.98 cm and a radius of 3.5 cm, and operates in the  $TE_{011}$  mode. The mode is excited with one of two coupling loops ( $\sim 3$  mm diameter) located  $180^\circ$  apart in the cavity midplane. The uncoupled  $Q$  is about 18 000. Large-diameter (1.4 cm) apertures in the center of the end caps are designed to allow as many of the atoms as possible to pass through the cavity. This increases the detection signal level, but at the expense of increased perturbation to the field structure.

The resonant microwave signal induces oscillations at the Rabi frequency given by Eq. (1). Ideally, the fraction of atoms expected in the  $|F=4\rangle$  state after passing through the cavity is given by

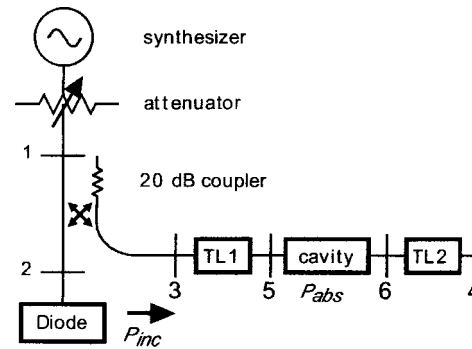


FIG. 3. Microwave measurement arrangement. Numbers 1 to 6 indicate reference planes used in the analysis. The cavity section includes the Ramsey cavity and the coupling to the cavity.

$$R = \frac{1 - \cos(\Omega_{R,\text{eff}} t_{\text{cav}})}{2}, \quad (2)$$

where  $t_{\text{cav}}$  is the time spent in the Ramsey cavity, and the effective Rabi frequency  $\Omega_{R,\text{eff}}$  is used to account for the variation in rf magnetic field strength with position in the cavity. For an ideal cavity without apertures, the ratio of  $\Omega_{R,\text{eff}}/\Omega_{R,\text{max}}$  is  $2/\pi$ , where  $\Omega_{R,\text{max}}$  is the Rabi frequency at the peak field location.

The amount of time spent in the cavity is set by the launch velocity or, alternatively, the toss height. The rf magnetic field strength in the cavity is controlled with a variable attenuator. Modifying the rf field strength is more easily achieved than changing the toss height, since the latter requires changing the timing of the entire toss sequence. In addition, the rf field strength can be changed over a wider dynamic range.

After the atoms pass through the Ramsey cavity on their way up, the microwave power to the cavity is turned off by means of an attenuator. Thus, the atoms are not exposed to any further microwave radiation as they complete the fountain motion and return. They therefore stay in the same quantum state until they reach the detection region. There they again encounter  $|F=4, m_F\rangle \Rightarrow |F'=5, m_F\rangle$  light, as illustrated in Fig. 1(a). Scattered photons of this light are detected and yield a signal proportional to the number of  $|F=4, m_F\rangle$  atoms. The light also removes the  $|F=4\rangle$  atoms. The  $|F=3\rangle$  atoms that remain then encounter a repump laser whose resonance is illustrated in Fig. 1(a). The repump laser puts the atoms into the  $|F'=4\rangle$  excited state, from which they fall back into the  $|F=4\rangle$  state, and they are then detected in the same manner. The fraction  $R$  of atoms in the  $|F=4\rangle$  state is given by  $R = N_4/(N_3 + N_4)$ , where  $N_3$  and  $N_4$  are the number of atoms in each state.  $R$  is calculated for each run and stored in a data file. Each data point presented is an average of 21 independent measurements.

## B. Microwave measurement apparatus

Microwave power is also measured by conventional techniques using the apparatus illustrated in Fig. 3. A diode power sensor monitored  $P_2$ , the power delivered to port 2 of a 20 dB coupler, while the Ramsey cavity and its transmission line feeds were connected to port 3 of the coupler. The diode sensor is a continuous-wave sensor of wide dynamic

range. Its nonlinearity is less than 3% as used in this experiment with its associated power meter. The proportionality constant between  $P_2$  and  $P_{inc}$ , the incident power at port 3, was determined by attaching a thin-film bolometric standard to port 3 in place of the fountain apparatus.  $P_{inc}$  during the Rabi oscillation experiment is then given by

$$P_{inc,m} = \frac{P_{sub} P_2 |1 - \Gamma_g \Gamma_s|^2}{CF_S P_{2S} |1 - \Gamma_g \Gamma_r|^2}, \quad (3)$$

where  $\Gamma_g$  is the equivalent generator reflection coefficient for port 3 for the coupler,  $\Gamma_s$  is the reflection coefficient of the standard,  $\Gamma_r$  is the reflection coefficient of the combined Ramsey cavity and transmission lines,  $P_{2S}$  is the power measured by the diode when the standard was attached,  $P_{sub}$  is the substituted power measured with the standard,  $CF_S$  is the calibration factor of the standard, and the  $m$  subscript on  $P_{inc,m}$  indicates the  $P_{inc}$  has been determined using conventional microwave techniques. The first ratio in Eq. (3) gives the incident power during the calibration. The last ratio in Eq. (3) is a mismatch factor that accounts for the power change due to changes in the constructive and destructive interference effects that occur when different devices are connected together.

The power delivered to the Ramsey cavity and diode is controlled with the attenuator between the source and port 1.  $P_{inc}$  during the experiment varied from about 100 pW to 300 nW. The measurement needs such low power levels partly because of the sensitivity of the measurement and partly because of the high- $Q$  resonant cavity. The enhanced sensitivity represents a significant advantage in a power measurement since it would allow for the use of a wider variety of transfer standards.

### III. VNA MEASUREMENTS

The experimental apparatus was not designed for microwave power measurements, and access to the Ramsey cavity is through semirigid cables with SMA connectors that have an electrical length of about 50 cm. The “TL” sections in Fig. 3 denote these cables. SMA components were not disconnected at any time, and adapters were used to establish reference planes with 3.5 mm connectors at ports 3 and 4. This was done so that the microwave measurements were performed at reference planes with metrology grade connectors. Port 4 was terminated by a short circuit during the Rabi oscillation experiment.

Microwave devices are typically characterized in terms of an  $N \times N$   $S$ -parameter matrix, where  $N$  is the number of ports on the device. For a two-port device with ports  $a$  and  $b$ , the diagonal terms  $S_{aa}$  and  $S_{bb}$  represent the reflection of the waves from each port, and the off-diagonal terms  $S_{ab}$  and  $S_{ba}$  represent transmission. Reciprocal devices like those used here have  $S_{ab} = S_{ba}$ . The  $S$  parameters are complex functions and contain information about both the amplitude and phase of the waves.

A commercial vector network analyzer (VNA) was used to measure the  $S$  parameters between ports 3 and 4. The VNA test ports were connected to ports 3 and 4 through nonstandard semirigid cables, since available conventional

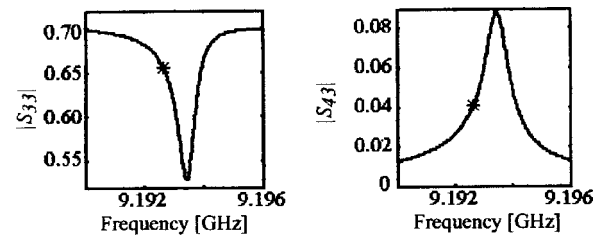


FIG. 4.  $|S_{33}|$  and  $|S_{43}|$  of the Ramsey cavity + transmission lines. Both are presented on a linear scale.

test cables were not long enough to reach the ports. The VNA measurements of  $|S_{33}|$  and  $|S_{43}|$  are shown in Fig. 4. The transmission-line losses in TL1 of Fig. 3 limit the maximum reflection coefficient to about 0.7 for  $|S_{33}|$ . The 3 dB bandwidth of  $|S_{43}|$  is about 780 kHz. When heated 5 °C above room temperature, the Ramsey cavity’s resonant frequency matches the cesium resonance at which the experiments were performed. Unfortunately, both the Rabi oscillation experiments and the VNA measurements were performed with an unheated cavity that had a resonant frequency of 9.1934 GHz. The asterisks in Fig. 4 show the value of  $|S_{33}|$  and  $|S_{43}|$  at the measurement frequency of 9.1926 GHz.

### IV. RABI OSCILLATION MEASUREMENTS

Data were taken for nominal toss heights of 32 and 45 cm. This represents the approximate upper and lower limits for the experiment. Since this means we have only two values of  $t_{cav}$  in Eq. (2), we demonstrate the Rabi oscillations by varying the power, and therefore,  $\Omega_{R,eff}$ , using the variable attenuator shown in Fig. 3. In Fig. 5(a), we plot the ratio  $R = N4/(N3+N4)$  [from Eq. (2)] versus  $(P_{inc,m})^{0.5}$ , which is proportional to the rf magnetic field strength. Rabi oscillations were clearly observed for both toss heights, including four cycles for the data with 32 cm toss height.

In order to compare the data for the 45 and 32 cm toss heights, we replot the data in Fig. 5(b) with the abscissa  $x$

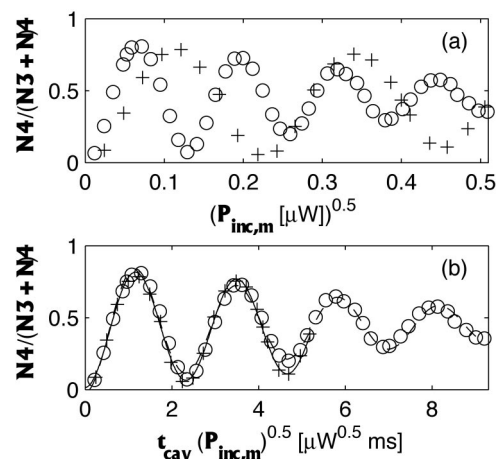


FIG. 5. Fraction of atoms in  $|F=4\rangle$  state after undergoing Rabi oscillations due to microwave radiation. (O and dashed line): 32 cm toss data; (+ and solid line): 45 cm toss data. (a) The  $x$  axis is proportional to the RF magnetic field. (b) The  $x$  axis is proportional to the time integral of the rf magnetic field seen by the atoms.

proportional to  $(P_{\text{inc},m})^{0.5} t_{\text{cav}}$ . This is proportional to the argument of the cosine in Eq. (2), and both sets of data should follow the same curve when plotted this way. There is a decay in the signal with increasing power, so the data were fit to functions that mimic Eq. (2), but also included an exponential damping factor. The fits are shown as lines in Fig. 5(b) and are best fits to  $y=y_0-a \exp(-x/d) \cos(kx)$ . In both cases, the key parameter related to the Rabi oscillation  $k$  has a standard uncertainty,  $u_k \leq 0.0045 k$ . This shows that the scaling with power level is as expected. In addition, the values of  $k$  from the two toss heights,  $k_{32}$  and  $k_{45}$ , agree very well with  $(k_{32}-k_{45})/\langle k \rangle = 0.0016$ , where  $\langle k \rangle$  is the average of the two values. This shows that the scaling with time is also as expected.

We have not identified a sole explanation for the decay of signal with power level. However, there are several factors that can explain at least some of the decay. One factor is that atoms that pass through the edge of the cavity's aperture see a weaker rf magnetic field than do atoms in the center. They undergo a smaller Rabi oscillation and the overall signal is reduced because there is a mixing of  $\Omega_{R,\text{eff}} t_{\text{cav}}$  phases. If the beam is uniformly distributed over the aperture, this effect produces a ratio of the third peak to the first peak of about 0.8. In comparison, the 32 cm toss data have a ratio of 0.5. A similar, but smaller effect is caused by the finite temperature of the cesium atoms. This produces a distribution of velocities and therefore  $t_{\text{cav}}$  values. A temperature of 7  $\mu\text{K}$  results in a value of 0.9 for the ratio of the third to first peaks. A third factor is that there is a finite probability for an atom to transition into an  $m_F \neq 0$  state. These atoms will stop oscillating and therefore reduce the signal level contrast.

## V. ABSOLUTE MEASUREMENT AND COMPARISON

### A. Absolute field measurement

The absolute value of the effective rf magnetic field  $H_{\text{eff}}$  can be obtained from the Rabi oscillation signal. At the first maximum in the oscillation,  $\Omega_{R,\text{eff}} t_{\text{cav}} = \pi$ , which corresponds to  $H_{\text{eff}} = \pi \hbar / (\mu_0 \mu_{\text{BG}} t_{\text{cav}} M)$ . For the 32 and 45 cm tosses, this yields  $H_{\text{eff}} = 1.57$  and  $2.77 \times 10^{-3}$  A/m, respectively. Note that these values of  $H_{\text{eff}}$  do not rely on the microwave measurements other than to help identify the peak signal location.

### B. Absolute comparison with traditional microwave measurement

We can obtain an incident power at port 3 from the Rabi oscillation measurement by evaluating a set of ratios

$$P_{\text{inc},R} = \frac{P_{\text{inc},3} P_{\text{abs}} W_{\text{cav}}}{P_{\text{abs}} W_{\text{cav}} H_{\text{eff}}^2} H_{\text{eff}}^2, \quad (4)$$

where  $W_{\text{cav}}$  is the energy stored in the cavity,  $P_{\text{abs}}$  is the power dissipated by the cavity and coupling structure, and the  $R$  subscript in  $P_{\text{inc},R}$  indicates that the power measurement is based on the Rabi oscillations. Calculation of the first ratio will be described below. The second ratio is given by  $P_{\text{abs}}/W_{\text{cav}} = \omega/Q_L$ , where  $Q_L$  is the loaded  $Q$  of the cavity. The third ratio has been estimated analytically by using the fields of a cavity without apertures.

TABLE I. Incident power at port 3 at the first peak in the Rabi oscillation as measured by the Rabi oscillations ( $P_{\text{inc},R}$ ) and by a traditional microwave measurement ( $P_{\text{inc},m}$ ).

Toss height (cm)	$P_{\text{inc},R}$ (nW)	$P_{\text{inc},m}$ (nW)
32	4.35	4.16
45	13.56	12.94

The first ratio and  $Q_L$  are obtained by use of the following  $S$ -parameter model:

$$S_{\text{TL1}} = \begin{bmatrix} 0 & e^{-\gamma_1 l_1} \\ e^{-\gamma_1 l_1} & 0 \end{bmatrix},$$

$$S_{\text{TL2}} = \begin{bmatrix} 0 & e^{-\gamma_2 l_2} \\ e^{-\gamma_2 l_2} & 0 \end{bmatrix},$$

and

$$S_{\text{cen,off}} = \begin{bmatrix} e^{-j\theta_1} & 0 \\ 0 & e^{-j\theta_2} \end{bmatrix}, \quad (5)$$

where  $S_{\text{TL1}}$  and  $S_{\text{TL2}}$  are matrices for the lossy transmission lines and  $S_{\text{cen,off}}$  is the off-resonant matrix for the Ramsey cavity plus coupling that is represented by the section between reference planes 5 and 6 in Fig. 3. The two key assumptions in the model are that the cavity reflects all power when off-resonance, and that the transmission-line reflection coefficients are zero. Calculations show that the on-resonance power absorbed between planes 5 and 6 is not dependent on the values of  $\theta_1$  or  $\theta_2$  in the third matrix, so we used  $\theta_1 = \theta_2 = 0$ . The values of  $\gamma_1$  and  $\gamma_2$  in Eq. (5) were obtained with a best fit to the off-resonant values of the measured  $S_{33}$  and  $S_{44}$ . Using this model for the transmission lines, the  $S$  parameters of the cavity and coupling structure between reference planes 5 and 6 are calculated as

$$S_{\text{cen,on}} = \begin{bmatrix} S_{55} & S_{56} \\ S_{65} & S_{66} \end{bmatrix} = \begin{bmatrix} S_{33} e^{2\gamma_1 l_1} & S_{34} e^{\gamma_1 l_1 + \gamma_2 l_2} \\ S_{43} e^{\gamma_1 l_1 + \gamma_2 l_2} & S_{44} e^{2\gamma_2 l_2} \end{bmatrix}. \quad (6)$$

Using standard techniques,<sup>8</sup> we obtained  $Q_L = 11\,430$  from fits to  $S_{56}$  and  $S_{55}$ . The first two matrices Eq. (5) and the matrix in Eq. (6) define a complete system that can then be used to solve for the power absorbed by the cavity and coupling structure between reference planes 5 and 6

$$\begin{aligned} \frac{P_{\text{abs}}}{P_{\text{inc},3}} &= e^{-2\alpha_1 l_1} - e^{2\alpha_1 l_1} \left| S_{33} - \frac{S_{34} S_{43}}{1 + S_{44}} \right|^2 - \frac{|S_{43}|^2}{|1 + S_{44}|^2} \\ &\quad \times (e^{2\alpha_2 l_2} - e^{-2\alpha_2 l_2}) \\ &\approx e^{-2\alpha_1 l_1} - e^{2\alpha_1 l_1} |S_{33}|^2, \end{aligned} \quad (7)$$

where  $\alpha_1 = \text{Re}(\gamma_1)$ . The dominant terms on the right can be obtained with a simple model using  $P_{\text{inc},5} = P_{\text{inc},3} e^{-2\alpha_1 l_1}$  and  $P_{\text{abs}} \approx P_{\text{inc},5} (1 - |S_{55}|^2)$ , or by assuming  $S_{43} \ll S_{33}$ .

Values for  $P_{\text{inc},R}$  obtained from Eq. (4) at the first peak in the Rabi oscillation curve (Fig. 5) are shown in Table I along with values obtained from the traditional microwave measurements. The two sets of numbers agree within 5%.

### C. Uncertainty in the Rabi-traditional measurement comparison

The largest source of uncertainty is due to uncertainties in the cavity temperature. The Rabi oscillation measurements in Fig. 5 and the VNA measurements in Fig. 4 were taken 3 days apart in a room in which the temperature was not well regulated. A rough estimate of the possible temperature change is 1 K, which places an upper bound on  $\Delta P_{\text{abs}}/P_{\text{abs}}$  of about 0.3 when evaluated using Eq. (7). Unfortunately, the small fountain experimental apparatus has not been available for additional measurements with better temperature control. Additional factors that could contribute uncertainties greater than 5% include the assumption that the transmission line segments produce no reflection, uncertainties in the measured  $S$ -parameter values, absorption of off-resonant power in the cavity coupling structure, effect of the cavity apertures, and determination of  $Q_L$ . No attempt has been made to characterize these uncertainties.

We conclude that the comparison between the Rabi oscillation measurement and a traditional microwave measurement agree within the rather large uncertainties in this experiment. These large uncertainties are not intrinsic to the Rabi oscillation measurement, but are an artifact of the existing apparatus that was adapted for this experiment. We hope to greatly reduce these uncertainties in the future by

designing and building an apparatus specifically intended for microwave power measurements.

### ACKNOWLEDGMENTS

The authors thank S. R. Jefferts for suggesting the use of the fountain apparatus for this experiment. D. X. LeGolvan, J. R. Juroshek, and J. L. McLean helped with the measurements. Helpful discussions with B. F. Riddle, M. D. Janezic, and J. R. Baker-Jarvis are also appreciated.

<sup>1</sup>A. Fantom, *Radio Frequency and Microwave Power Measurement* (Peregrinus, London, 1990).

<sup>2</sup>R. C. Mockler, *Adv. Electron. Electron Phys.* **15**, 1 (1961).

<sup>3</sup>T. P. Heavner, S. R. Jefferts, E. A. Donley, and T. E. Parker, *Proc. IEEE Intl. Frequency Control Symp. and PDA Exhibition*, New Orleans, LA, 29–31 May 2002, pp. 473–475.

<sup>4</sup>T. P. Crowley, E. A. Donley, T. P. Heavner, J. R. Juroshek, and B. F. Riddle, *IEEE MTT-S Intl. Microwave Symp. Digest*, Philadelphia, PA, 8–13 June 2003, Vol. 2, pp 1427–1430.

<sup>5</sup>E. A. Donley, T. P. Crowley, T. P. Heavner, and B. F. Riddle, *Proc. IEEE Intl. Frequency Control Symp. and PDA Exhibition*, Tampa, FL, 4–8 May 2003, pp. 135–137.

<sup>6</sup>D. Paulusse, N. Rowell, and A. Michaud, *Proc. Conf. On Precision Electromagnetic Measurements*, Ottawa, Ontario, Canada 16–21 June 2002, pp. 194–195.

<sup>7</sup>H. J. Metcalf and P. van der Straten, *Laser Cooling and Trapping* (Springer, New York, 1999).

<sup>8</sup>D. Kajfez, *IEEE Trans. Microwave Theory Tech.* **MTT-42**, 1149 (1994).